Geophysical Research Letters

RESEARCH LETTER
10.1029/2018GL081170

Key Points:
- Single-crystal X-ray diffraction experiments were carried out on high-Fe and low-Fe eclogitic garnets and omphacites to 24 GPa and 700 K
- Metastable low-Fe eclogite may contribute to the slab stagnation in the upper range of the transition zone
- Eclogite can explain density anomalies at depths of 100–200 km in the upper mantle of Asia

Supporting Information:
- Supporting Information S1
- Table S8
- Table S6
- Table S2

Correspondence to:
D. Fan and P. Dera,
fandawei@vip.gyig.ac.cn;
pdera@hawaii.edu

Citation:
Xu, J., Zhang, D., Fan, D., Dera, P. K., Shi, F., & Zhou, W. (2019). Thermoelastic properties of eclogitic garnets and omphacites: Implications for deep subduction of oceanic crust and density anomalies in the upper mantle. *Geophysical Research Letters*, *46*, 179–188. https://doi.org/10.1029/2018GL081170

Received 2 NOV 2018
Accepted 27 DEC 2018
Accepted article online 2 JAN 2019
Published online 15 JAN 2019

Thermoelastic Properties of Eclogitic Garnets and Omphacites: Implications for Deep Subduction of Oceanic Crust and Density Anomalies in the Upper Mantle

Jingui Xu[1,2], Dongzhou Zhang[2], Dawei Fan[1], Przemyslaw K. Dera[2], Feng Shi[3], and Wenge Zhou[1]

[1]Key Laboratory of High-Temperature and High-Pressure Study of the Earth's Interior, Institute of Geochemistry, Chinese Academy of Sciences, Guiyang, China, [2]Hawaii Institute of Geophysics and Planetology, School of Ocean and Earth Science and Technology, University of Hawai'i at Mānoa, Honolulu, HI, USA, [3]State Key Laboratory of Geological Processes and Mineral Resources, China University of Geoscience, Wuhan, China

Abstract Synchrotron-based high-pressure/high-temperature single-crystal X-ray diffraction experiments to ~24 GPa and 700 K were conducted on eclogitic garnets (low-Fe: $Prp_{28}Alm_{38}Grs_{33}Sps_1$ and high-Fe: $Prp_{14}Alm_{62}Grs_{19}Adr_3Sps_2$) and omphacites (low-Fe: $Quad_{57}Jd_{42}Ae_1$ and high-Fe: $Quad_{53}Jd_{27}Ae_{20}$), using an externally heated diamond anvil cell. Fitting the pressure-volume-temperature data to a third-order Birch-Murnaghan equation of state yields the thermoelastic parameters including bulk modulus (K_{T0}), its pressure derivative (K'_{T0}), temperature derivative ($(\partial K_T/\partial T)_P$), and thermal expansion coefficient (α_T). The densities of the high-Fe and low-Fe eclogites were then modeled along typical geotherms of the normal mantle and the subducted oceanic crust to the transition zone depth (550 km). The metastable low-Fe eclogite could be a reason for the stagnant slabs within the upper range of the transition zone. Eclogite would be responsible for density anomalies within 100–200 km in the upper mantle of Asia.

Plain Language Summary Eclogite mainly consists of pyrope-almandine-grossular garnet and sodium-rich pyroxene (omphacite) and is a key component of the Earth's upper mantle and oceanic crust. It plays an important role in the mantle convection. The lack of thermoelastic parameters of eclogitic garnets and omphacites hampers accurate modeling of eclogite density at deep-Earth pressure-temperature conditions. In this study, we obtained the thermoelastic parameters of natural eclogitic garnets and omphacites and then modeled the densities of high-Fe and low-Fe eclogites in the subducted oceanic crust and the normal upper mantle. In the upper mantle, eclogite enhances the slab subduction into the transition zone; however, the presence of the metastable low-Fe eclogite would promote the slab stagnation within the upper range of the transition zone. Additionally, eclogite can explain positive density anomalies at depths of 100–200 km of the upper mantle of Asia identified by seismic observations.

1. Introduction

Eclogite is an important high-pressure metamorphic rock and mainly forms from basalt or gabbro in the subducting slab (Ringwood, 1982). Eclogite is mainly composed of garnet and omphacite and plays a key role in mantle convection due to its relatively high density (Anderson, 2006; Aoki & Takahashi, 2004; Irifune et al., 1986). In addition, the occurrences of eclogitic xenoliths in kimberlites and solid inclusions in diamonds indicate the presence of eclogite in the mantle (e.g., Jacob, 2004; Taylor et al., 1996). Eclogite may explain positive density anomalies in the upper mantle (Mooney & Kaban, 2010), for instance, the widespread density anomalies of Asia at depths of 100–200 km beneath the Tarim basin, Himalayas, and Siberian craton (Kaban, Khrepy, et al., 2016; Kaban, Stolk, et al., 2016).

Natural eclogitic omphacite and garnet are found as minerals with complex composition, which are generally described as a solid solution of multiple pyroxene and garnet end-members, respectively. Omphacite is a clinopyroxene mineral with a composition intermediate between jadeite (Jd, $NaAlSi_2O_6$) and diopside (Di, $CaMgSi_2O_6$) but often has other components of aegirine (Ae, $NaFe^{3+}Si_2O_6$) and

hedenbergite (Hd, $CaFeSi_2O_6$). It has monoclinic symmetry with $C2/c$ or $P2/n$ space group depending on crystallization conditions, and the $C2/c$-$P2/n$ transition takes place at ~1000 K at 1 bar (Fleet et al., 1978). Like other pyroxenes, the general crystal-chemical formula of omphacite can be described as $M2M1T_2O_6$, where M2 and M1 are two different octahedral sites, and T are tetrahedral sites. Commonly, M2 sites are occupied by Ca^{2+} and Na^{+} cations, M1 sites are filled with Mg^{2+}, Fe^{2+}, Fe^{3+}, and Al^{3+}, while T sites are occupied predominantly by Si^{4+}, but can contain small quantities of Al^{3+}.

Garnet has cubic symmetry with $Ia\bar{3}d$ space group, and numerous studies have described the garnet structure in great detail (e.g., Geiger, 2013). Its general crystal-chemical formula is commonly represented as $X_3Y_2Z_3O_{12}$, where Z are tetrahedral sites mostly occupied by Si^{4+}; Y are octahedral cation sites, usually filled with Al^{3+}, Fe^{3+} and Cr^{3+}; X cations are coordinated by eight oxygen atoms and can accommodate Mg^{2+}, Fe^{2+}, Ca^{2+}, Mn^{2+}, and so on. Eclogites incorporated as xenoliths in eruptive rocks from global major ultrahigh-pressure metamorphic (UHPM) belts and kimberlites indicate that eclogitic garnets are mainly composed of pyrope (Prp, $Mg_3Al_2Si_3O_{12}$), almandine (Alm, $Fe_3Al_2Si_3O_{12}$) and grossular (Grs, $Ca_3Al_2Si_3O_{12}$) with very few other end-member garnets like spessartine (Sps, $Mn_3Al_2Si_3O_{12}$) and andradite (Adr, $Ca_3Fe^{3+}{}_2Si_3O_{12}$; e.g., Kosman et al., 2016; Ren et al., 2017; Taylor et al., 1996; Wang, 1998; Wang et al., 2009; Weber & Bucher, 2015). In addition, some eclogitic garnets generally contain ~1 wt.% of TiO_2 (e.g., Stachel & Harris, 2008; Wang et al., 2009), which could be neglected in that case, although some studies reported garnets with high Ti content (Wang et al., 2009), in which case the present model may not be applicable.

Understanding the thermoelastic properties of eclogitic garnet and omphacite is important to model the structure and fate of the subducted slab in the upper mantle (e.g., Bass & Anderson, 1984; Bass & Parise, 2008; Duffy & Anderson, 1989; Frost, 2008). A number of studies have been conducted on the thermoelastic properties of end-member garnets (e.g., Arimoto et al., 2015; Fan, Xu, Ma, Wei, et al., 2015; Gréaux et al., 2011; Hu et al., 2016; Wang et al., 1998; Zhang et al., 1999) and binary garnet solutions including Prp-Alm, Alm-Sps, Grs-Adr, and Prp-Grs (Du et al., 2015; Fan et al., 2011; Fan, Xu, Ma, Liu, et al., 2015; Fan et al., 2017; Huang & Chen, 2014; Milani et al., 2015). However, studies on thermoelastic behaviors of ternary garnets at simultaneously high-pressure (P)/high-temperature (T) conditions are limited. There has been only one experimental study on the thermoelastic properties of Prp-Alm-Grs garnet ($Prp_{68}Alm_{24}Grs_5Sps_1$; Lu et al., 2013), and the grossular content was significantly lower than that of common eclogitic garnets (typically, eclogitic garnets have Grs contents larger than 20 mol%; Stachel & Harris, 2008). Additionally, the mixing properties of Prp-Alm-Grs ternary garnets are suggested to be nonideal (Ganguly et al., 1993; Geiger et al., 1987; Koziol & Newton, 1989), which may prevent from using a monotonic relation to recalculate the elastic properties of the solid solution from those of the end-members. Therefore, previous studies have not fully constrained the thermoelastic properties of eclogitic garnets.

Studies on the elastic properties omphacite at room T have been conducted extensively (e.g., Pandolfo et al., 2012a; Pandolfo et al., 2012b; Pavese et al., 2001; Zhang et al., 2016), yet studies at high-P/high-T conditions are limited (Nishihara et al., 2003; data collected to 10 GPa and 1000 K). Like other pyroxenes, omphacite was expected to dissolve into garnet as the oceanic crust descends into the mantle (Akaogi & Akimoto, 1977). However, recent studies indicated that the pyroxene-garnet reaction was inhibited under cold subduction zone conditions; thus, eclogitic omphacite and garnet are expected to be preserved in subducted oceanic crust to transition zone depths (Nishi et al., 2008, 2009, 2013; Van Mierlo et al., 2013). Therefore, it is necessary to explore the thermoelastic behaviors of eclogitic omphacite and garnet at high P-T to pressures higher than 10 GPa.

Here we reported the thermal equation of state (EoS) of natural high-Fe and low-Fe eclogitic garnets and omphacites at high-P/high-T conditions to ~24 GPa and 700 K using synchrotron single-crystal X-ray diffraction (XRD) coupled with an externally heated diamond anvil cell. Using the obtained thermoelastic parameters of these eclogitic garnets and omphacites, we discussed the effects of composition on the elastic properties of eclogitic garnet and omphacite. We also used these thermoelastic parameters to model the density of eclogite in the normal upper mantle and oceanic crust. Finally, we applied these results to discuss potential geophysical implications of eclogite for the dynamics of the subduction zone and the upper mantle.

2. Materials and Methods

Natural garnets and omphacites were collected from eclogite in Dabie-Sulu UHPM belt (supporting information Text S1). The chemical compositions of garnets were obtained as $Prp_{28}Alm_{38}Grs_{33}Sps_1$ (low Fe) and $Prp_{14}Alm_{62}Grs_{19}Adr_3Sps_2$ (high Fe), while the compositions of two omphacites were $Quad_{57}Jd_{42}Ae_1$ (low Fe; Quad indicates Ca-Mg-Fe pyroxenes; Morimoto, 1988) and $Quad_{53}Jd_{27}Ae_{20}$ (high Fe; Table S1). Single-crystal XRD experiments were carried out at experimental station 13-BM-C of the Advanced Photon Source, Argonne National Laboratory (Fei et al., 2007; Kantor et al., 2012; Rivers et al., 2008; Zhang et al., 2017) (supporting information Text S2). The GSE_ADA/RSV software (Dera et al., 2013) was used to analyze the diffraction data (Figure S1). Data analyses of the single-crystal XRD patterns indicate that omphacite $Quad_{57}Jd_{42}Ae_1$ has $C2/c$ space group, while $Quad_{53}Jd_{27}Ae_{20}$ has $P2/n$. The unit-cell parameters of garnets and omphacites at various P–T conditions are given in Tables S2–S4, and there was no evidence of phase transitions throughout the P–T range studied.

3. Results and Discussion

3.1. EoS of Eclogitic Garnets and Omphacites

The room-T unit-cell volumes of eclogitic garnets and omphacites undergo nonlinear decreases with no discontinuity in the compression curves up to the maximum pressure, as shown in Figures S2–S5. The pressure-volume (P-V) data were fitted using a third-order Birch-Murnaghan EoS (BM3-EoS) to obtain the elastic parameters zero-P unit-cell volume (V_0), isothermal bulk modulus (K_0), and its pressure derivative (K'_0), using the program EoSFit7c (Angel et al., 2014; Gonzalez-Platas et al., 2016). The results were compared with those derived from the fittings by a second-order Birch-Murnaghan EoS (BM2-EoS) and the Vinet EoS (Vinet et al., 1986). The obtained results of these elastic parameters (Table S5) were assessed by various strategies like the confidence ellipses of the coefficient between K_0 and K'_0 (Figures S6 and S8), the F_E-f_E plot (Figures S7 and S9), and the comparison between the refined and measured values of V_0 (e.g., Angel, 2000; Bass et al., 1981). Finally, we concluded that the BM3-EoS is a reasonable choice for fitting the P-V data of $Prp_{28}Alm_{38}Grs_{33}Sps_1$, $Prp_{14}Alm_{62}Grs_{19}Adr_3Sps_2$, and $Quad_{53}Jd_{27}Ae_{20}$, while the P-V data of $Quad_{57}Jd_{42}Ae_1$ can be reasonably described by the BM2-EoS (supporting information Text S3).

The pressure-volume-temperature (P-V-T) data (Figure 1) were fitted using the high-temperature BM3-EoS (HT-BM3-EoS) to obtain the thermoelastic parameters (Table 1) V_0, K_{T0}, K'_{T0}, thermal expansion coefficient (α_T), and the temperature derivative of K_{T0} ($(\partial K_T/\partial T)_P$) (supporting information Text S4).

3.2. Comparisons With Previous Studies

3.2.1. Garnets

The elastic parameters K_0 and K'_0 of eclogitic garnets were compared with other aluminosilicate garnets (Table S6). The K'_0 values of eclogitic garnets (4.3(2) for $Prp_{28}Alm_{38}Grs_{33}Sps_1$ and 5.0(2) for $Prp_{14}Alm_{62}Grs_{19}Adr_3Sps_2$) are roughly within the ranges of the values of end-member garnets (Prp: 4.4–6.4, Alm: 4.2–5.8, and Grs: 5.0–5.2; e.g., Levien et al., 1979; Milani et al., 2015; Zhang et al., 1999; Zou et al., 2012). However, the K_0 values are smaller. With fixed K'_0 at 4, the K_0 values from XRD studies are 171–176, 178–186, and 166–176 GPa for Prp, Alm, and Grs, respectively. These are larger than those of the eclogitic garnets (163.6(5) and 164.8(5) GPa for $Prp_{28}Alm_{38}Grs_{33}Sps_1$ and $Prp_{14}Alm_{62}Grs_{19}Adr_3Sps_2$, respectively). Additionally, the K_0 values obtained by Brillouin scattering spectroscopy (BLS) and ultrasonic interferometry (UI; 169–174, 173, and 167–170 GPa for Prp, Alm, and Grs, respectively) are also larger than those of the eclogitic garnets (Chen et al., 1999; Gwanmesia et al., 2006; Isaak et al., 1992; Jiang et al., 2004; Kono et al., 2010; Leitner et al., 1980; O'Neill et al., 1991; Sinogeikin & Bass, 2000, 2002; Skinner, 1956; Soga, 1967; Sumino & Nishizawa, 1978; Verma, 1960; Webb, 1989). Therefore, the eclogitic garnets have smaller K_0 values than the end-member garnets Prp, Alm, and Grs. As shown in Figure S10, the compressional curves indicate that two eclogitic garnets are more compressible than the end-member garnets.

The K_0 values of the eclogitic garnets were also compared with those of other Prp-Alm-Grs garnets. Most Prp-Alm-Grs garnets in previous studies (BLS and UI) contain Grs content less than 10 mol%, and the K_0 values are 167–176 GPa and larger than those of our eclogitic garnets. It should be noted that the smaller K_0 value of $Prp_{14}Alm_{62}Grs_{19}Adr_3Sps_2$ could result from the incorporation of Adr, as Adr has a smaller K_0 value (157(2) GPa; Bass, 1986; Zhang et al., 1999) than Prp, Alm, and Grs. However, the addition of

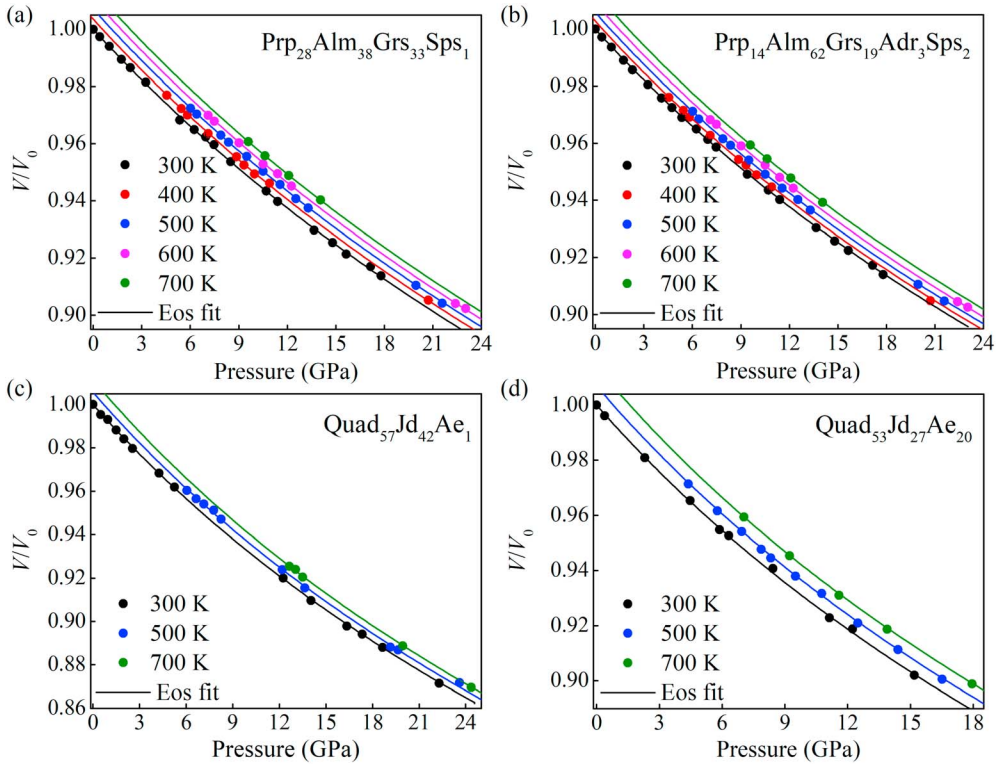

Figure 1. Pressure-volume-temperature relations of eclogitic garnets ([a] $Prp_{28}Alm_{38}Grs_{33}Sps_1$ and [b] $Prp_{14}Alm_{62}Grs_{19}Adr_3Sps_2$) and omphacites ([c] $Quad_{57}Jd_{42}Ae_1$ and [d] $Quad_{53}Jd_{27}Ae_{20}$). Isothermal compression curves are calculated by using the obtained thermoelastic parameters of this study.

1 mol% Sps may not lower the K_0 of $Prp_{28}Alm_{38}Grs_{33}Sps_1$, as the K_0 value of Sps (172–179 GPa; Bass, 1989; Babuška et al., 1978) is comparable to that of other end-member garnets. Therefore, other reasons should be considered (see the following paragraph).

The K_0 values of Prp-Alm, Alm-Sps and Grs-Adr solid solutions change linearly with the composition (Huang & Chen, 2014; Fan, Xu, Ma, Liu, et al., 2015; Fan et al., 2017). However, the K_0 values along the Prp-Grs solid solution show a nonlinear compositional dependence, and the garnets with intermediate compositions have smaller K_0 values than the end-members, due to the large positive excess volume (Du et al., 2015). The incorporation of Grs into the Prp-Alm solution may also result in excess volume for Prp-Alm-Grs garnets (Koziol & Newton, 1989) and cause a smaller K_0 value of $Prp_{28}Alm_{38}Grs_{33}Sps_1$ compared to those of end-member garnets. Previous studies obtained larger K_0 values (167–176 GPa) for Prp-Alm-Grs garnets with less than 3 mol% Grs (Table S6), which may indicate that this minor Grs content has little effects on K_0. Recently, a high-pressure XRD study was conducted on a Prp-Alm-Grs garnet ($Prp_{51}Alm_{22}Grs_{27}$) and provided a K_0 value of 166(2) GPa (Milani, 2015), which is larger than that of $Prp_{28}Alm_{38}Grs_{33}Sps_1$ (as indicated by Figure S10) and more comparable to those values of low-Grs Prp-Alm-Grs garnets. It seems that increasing Grs content in Prp-Alm-Grs garnets decreases the K_0 value. Along the Prp-Alm solid solution, the K_0 value increases with increasing Alm content (Huang & Chen, 2014; Milani et al., 2015). However,

Table 1
Thermoelastic Parameters Derived From the Fitting of P-V-T Data to the HT-BM3-EoS

Composition	V_0 (Å^3)	K_{T0} (GPa)	$K_{T}'_0$	$(\partial K_T/\partial T)_P$ (GPa/K)	α_0 (10^{-5} K^{-1})	α_1 (10^{-8} K^{-2})
$Prp_{28}Alm_{38}Grs_{33}Sps_1$	1570.2(2)	162(1)	4.3(2)	−0.010(7)	3.5(4)	0.1(8)
$Prp_{14}Alm_{62}Grs_{19}Adr_3Sps_2$	1564.9(1)	159.0(9)	5.0(2)	−0.010(4)	1.7(2)	2.9(5)
$Quad_{57}Jd_{42}Ae_1$	422.3(1)	123.6(5)	4^{fixed}	−0.011(5)	2.8(3)	—
$Quad_{53}Jd_{27}Ae_{20}$	426.0(2)	115(2)	4.9(4)	−0.009(6)	3.4(4)	—

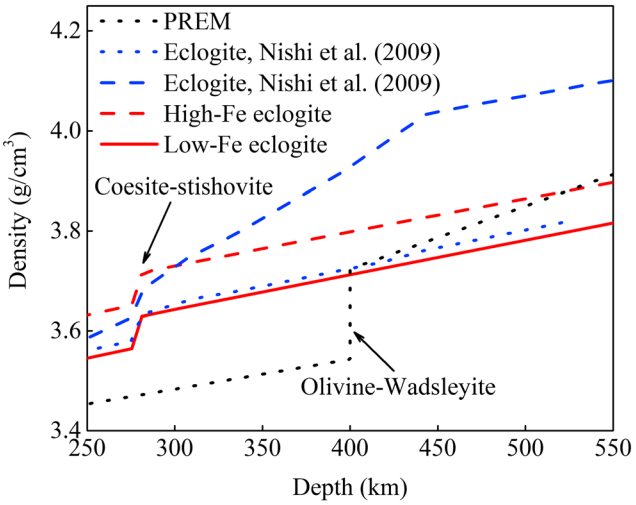

Figure 2. Density for eclogite along a geotherm (Eberle et al., 2002) of the subducting oceanic crust and the seismic model PREM (Dziewonski & Anderson, 1981) is also shown. The blue dotted line represents the density of untransformed eclogite from Nishi et al. (2009). The blue dashed line represents the density of eclogite from Nishi et al. (2009) that involves the formation of majorite by absorption of clinopyroxene. The red dashed and solid lines represent the metastable high-Fe and low-Fe eclogite, respectively. High-Fe eclogite: mineral assemblage of 20 vol% $Prp_{14}Alm_{62}Grs_{19}Adr_3Sps_2$, 75 vol% $Quad_{53}Jd_{27}Ae_{20}$, and 5 vol% coesite/stishovite; low-Fe eclogite: mineral assemblage of 20 vol% $Prp_{28}Alm_{38}Grs_{33}Sps_1$, 75 vol% $Quad_{57}Jd_{42}Ae_1$, and 5 vol% coesite/stishovite.

when Grs joins, the changes of K_0 values of Prp-Alm garnets with composition become complicated, which resembles the behavior of the Prp-Grs solution (Du et al., 2015).

The thermoelastic parameters α_{300K} and $(\partial K_T/\partial T)_P$ of eclogitic garnets were also compared to those of previous HT-BM-EoS studies on end-member garnets Prp, Alm, and Grs (Table S7). Like the bulk modulus, the values of $(\partial K_T/\partial T)_P$ for both eclogitic garnets (−0.010(7) and −0.010(4) GPa/K for $Prp_{28}Alm_{38}Grs_{33}Sps_1$ and $Prp_{14}Alm_{62}Grs_{19}Adr_3Sps_2$, respectively) are smaller than those of end-member garnets (−0.018(2)−−0.043(14) GPa/K). In this study, two eclogitic garnets have comparable values of $(\partial K_T/\partial T)_P$, which may indicate that the compositional effect on the $(\partial K_T/\partial T)_P$ value of Prp-Alm-Grs garnet solutions is limited. For the thermal expansion α_{300K}, $Prp_{28}Alm_{38}Grs_{33}Sps_1$ ($3.5(6)\times10^{-5}$ K^{-1}) has a larger value than those of end-member garnets Prp (2.6(3)-3.0(3) $\times10^{-5}$ K^{-1}), Alm ($3.3(9)\times10^{-5}$ K^{-1}), and Grs ($2.8(2)\times10^{-5}$ K^{-1}). However, the α_{300K} value of $Prp_{14}Alm_{62}Grs_{19}Adr_3Sps_2$ ($2.6(4)\times10^{-5}$ K^{-1}) is more comparable to that of the end-member garnets and smaller than that of $Prp_{28}Alm_{38}Grs_{33}Sps_1$. Therefore, for Prp-Alm-Grs solution, the compositional effects on the thermal expansion should be considered, and the increasing Alm content may lower the thermal expansion.

3.2.2. Omphacites

The K_0 and K'_0 values of two eclogitic omphacites were compared to previous studies on omphacites and relevant end-member clinopyroxenes including Di, Jd, Hd, and Ae (Table S8). In contrast to garnets, very few of these results are from BLS or UI experiments (Bhagat et al., 1992; John & Weidner, 1988; Kandelin & Weidner, 1988; Li & Neuville, 2010; Sang & Bass, 2014; Stixrude & Lithgow-Bertelloni, 2011; Tribaudino et al., 2008), and most are obtained by the XRD method (e.g., Gavrilenko et al., 2010; Levien & Prewitt, 1981; McCarthy, Downs, Thompsom, & Redhammer, 2008; Nestola et al., 2006; Posner et al., 2014; Thompson & Downs, 2008; Xu et al., 2017; Zhang et al., 1997; Zhao et al., 1997, 1998) (Table S8).

The K'_0 values are within the range of end-member clinopyroxenes (K'_0 = 3.2–6.2; Table S8). With fixed $K'_0 = 4$, the K_0 values of $Quad_{57}Jd_{42}Ae_1$ (123.6(5) GPa) and $Quad_{53}Jd_{27}Ae_{20}$ (120.3(9) GPa) are larger than those of Di (110–117 GPa), Hd (117 GPa), and Ae (113–120 GPa), but smaller than those of Jd (127–134 GPa; Table S8 and Figure S11).

Additionally, the K_0 values of two eclogitic omphacites were also compared to those of previous EoS studies on omphacites (Figures S11 and S12), also with fixed $K'_0 = 4$. As shown in Figure S11, the K_0 value of omphacite increases with the Jd content as proposed by Pandolfo et al. (2012b), as other end-member clinopyroxenes like Di, Hd, and Ae have comparable K_0 values that are significantly smaller than that of Jd (Table S8). The notably large K_0 of Nishihara et al. (2003; $Quad_{72}Jd_{28}$) may result from its high contents (~13 mol%) of $CaAl_2SiO_6$, as the effective ionic radius of six-coordinated Al^{3+} (0.535 Å) is smaller than that of Mg^{2+} (0.720 Å; Shannon, 1976) and smaller cations cause lower compressibilities for clinopyroxenes (e.g., McCarthy, Downs, & Thompson, 2008). Pavese et al. (2001) obtained a smaller K_0 value of $Quad_{49}Jd_{45}Ae_6$ that might suffer from the presence of non-hydrostatic conditions at high pressures, as they employed nitrogen as the pressure-transmitting medium (the presence of non-hydrostatic stress occurs at ~3 GPa; Angel et al., 2007). The discrepancy of K_0 values between Zhang et al. (2016; $Quad_{52}Jd_{44}Ae_4$) and this study ($Quad_{57}Jd_{42}Ae_1$) is likely due to the different experimental pressure ranges; the maximum pressure is much higher (47 GPa) in the former.

Table S9 summarizes the thermoelastic parameters α_{300K} and $(\partial K_T/\partial T)_P$ of Di, Jd, and omphacites, which are derived from the fitting of the *P-V-T* data to the HT-BM-EoS. The α_{300K} value of $Quad_{57}Jd_{42}Ae_1$ ($2.8(3)\times10^{-5}$ K^{-1}) is comparable to those of Di ($2.9(1)\times10^{-5}$ K^{-1}), Jd ($2.6(3)\times10^{-5}$ K^{-1}), and $Quad_{72}Jd_{28}$ ($2.7(3)\times10^{-5}$ K^{-1}) but smaller than that of $Quad_{53}Jd_{27}Ae_{20}$ ($3.4(4)\times10^{-5}$ K^{-1}). Therefore, increasing Ae content may enhance the thermal expansion of omphacite, while there may be little effects

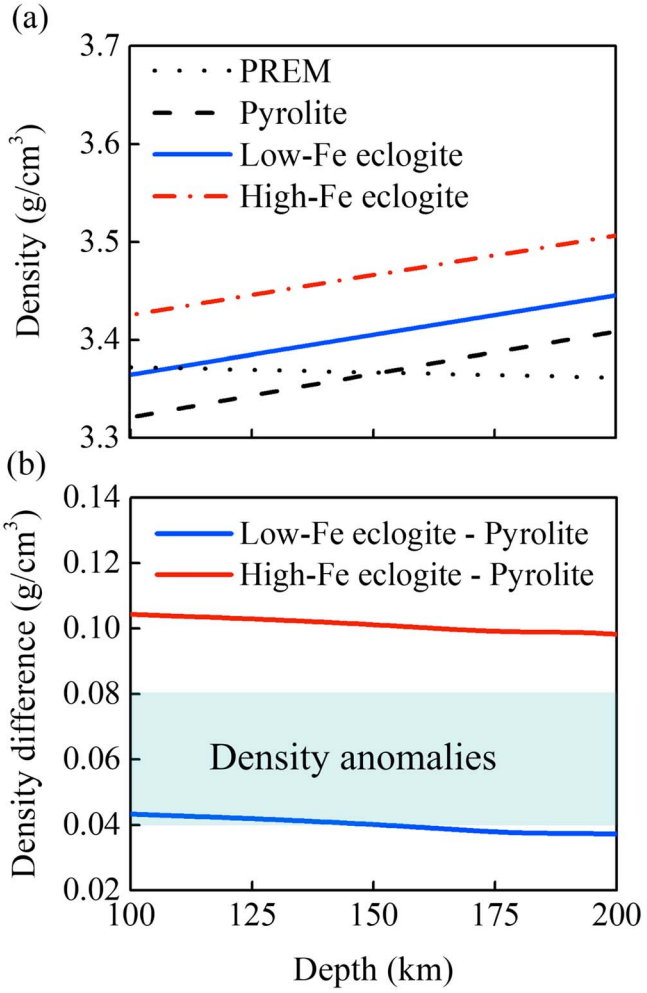

Figure 3. (a) Density profiles of eclogite assemblages along a normal mantle geotherm (Katsura et al., 2010). The seismic model PREM is from Dziewonski and Anderson (1981), and the density profile of the pyrolite is obtained from Cammarano et al. (2003). (b) Density difference between eclogite and pyrolite. The colored region indicates the density anomalies in the upper mantle of Asia at depths of 100–200 km. High-Fe eclogite: mineral assemblage of 20 vol% $Prp_{14}Alm_{62}Grs_{19}Adr_3Sps_2$, 75 vol% $Quad_{53}Jd_{27}Ae_{20}$, and 5 vol% coesite; low-Fe eclogite: mineral assemblage of 20 vol% $Prp_{28}Alm_{38}Grs_{33}Sps_1$, 75 vol% $Quad_{57}Jd_{42}Ae_1$, and 5 vol% coesite.

from the variations of other components like Jd and Di. In comparison with the thermal expansion, the compositional effects on the $(\partial K_T/\partial T)_P$ may be smaller. In this study, the $(\partial K_T/\partial T)_P$ values of $Quad_{57}Jd_{42}Ae_1$ (−0.011(5) GPa/K) and $Quad_{53}Jd_{27}Ae_{20}$ (−0.009(6) GPa/K) are comparable. These values are also comparable to that of Jd (−0.014(5) GPa/K) but smaller than those of Di (−0.021(4) GPa/K) and $Quad_{72}Jd_{28}$ (−0.026(5) GPa/K).

4. Geophysical Implications

Eclogite has been proposed as the driving force for subduction after the basalt-eclogite transition within the oceanic crust (e.g., Ringwood, 1982). In addition, eclogite in the upper mantle has been generally interpreted as remnants of ancient subduction (e.g., Jacob, 2004) and considered as a cause of some density anomalies within 100–200 km (Kaban, Khrepy, et al., 2016; Kaban, Stolk, et al., 2016). Therefore, to better understand the role of eclogite in both subduction and normal upper mantle, we modeled the density of eclogite along the geotherms of the oceanic crust (Eberle et al., 2002) and the normal upper mantle (Katsura et al., 2010). During the calculation, we used the HT-BM3-EoS and the obtained thermoelastic parameters of eclogitic garnets and omphacites. In this model, the eclogite consists of 20 vol% garnet, 75 vol% omphacite, and 5 vol% coesite (Nishi et al., 2009), and the densities of eclogite assemblages are estimated by using a Voigt-Reuss-Hill average (Hill, 1952). This model assumes that the eclogitic garnets and omphacites metastably survive to 550 km, while the coesite-stishovite transition occurs at ~9 GPa (Nishi et al., 2009). The used thermoelastic parameters of eclogitic garnets and omphacites (this study) and coesite and stishovite are shown in Table S10.

4.1. Eclogite and the Slab Subduction

The densities of high-Fe ($Prp_{14}Alm_{62}Grs_{19}Adr_3Sps_2$ + $Quad_{53}Jd_{27}Ae_{20}$ + coesite) and low-Fe ($Prp_{28}Alm_{38}Grs_{33}Sps_1$ + $Quad_{57}Jd_{42}Ae_1$ + coesite) eclogites in the subducted oceanic crust are shown in Figure 2. The density of metastable eclogite with Mid-ocean ridge basalt (MORB) composition from Nishi et al. (2009) is also shown in Figure 2, which is higher than that of the low-Fe eclogite by 0.4% at ~300 km but lower than that the high-Fe eclogite by 2.3% at ~300 km. Compared with the eclogite involving the formation of majorite (Figure 2), these metastable eclogites have lower densities at depths of 300–550 km.

Density is an important factor controlling the sinking or stagnation of the slabs (Agrusta et al., 2014). As shown in Figure 2, in the upper mantle, the metastable eclogites are denser than the Preliminary reference Earth model (PREM), indicating the higher density of eclogite provides a plunging force to the slab. The high-Fe eclogite is denser than the PREM mantle up to ~520 km, which indicates that the presence of high-Fe eclogite would facilitate the slab to sink into the middle range of the transition zone. However, the low-Fe eclogite has a lower density than the PREM after entering the transition zone, indicating that the presence of low-Fe eclogite would enhance the slab stagnation within the upper range of the transition zone. Indeed, seismic observations have demonstrated some stagnant slabs within the upper range of the transition zone, which are located beneath the Peruvian continental arc, the eastern Java arc, the southern Kurile arc, and so on (Fukao et al., 2001; Fukao & Obayashi, 2013).

4.2. Eclogite and the Positive Density Anomalies in the Upper Mantle

Recently, some positive density anomalies at depths of 100–200 km of the upper mantle of Asia (beneath the Tarim, Himalayas, South China craton, South Urals, etc.) were identified by geophysical observations

(Kaban, Khrepy, et al., 2016; Kaban, Stolk, et al., 2016). These anomalies have values between 0.04 and 0.08 g/cm^3 and are explained by the presence of eclogite bodies (Kaban, Khrepy, et al., 2016; Kaban, Stolk, et al., 2016). To verify the reasonability, the densities of the high-Fe and low-Fe eclogites at depths of 100–200 km along a normal mantle geotherm were calculated. As shown in Figure 3a, the densities of both eclogites are compared with those of the pyrolite (Cammarano et al., 2003) that is thought to be a representative rock of the upper mantle.

The high-Fe eclogite is denser than the pyrolite by ~0.10 g/cm^3, while the density difference between low-Fe eclogite and pyrolite is ~0.04 g/cm^3 (Figure 3b). Therefore, the low-Fe eclogite can explain the density anomalies beneath the South Urals and Siberian craton where the anomalies are 0.04–0.06 g/cm^3. However, density anomalies with larger values like those beneath the Tarim and Himalayas (larger than 0.06 g/cm^3) may result from eclogites with higher Fe contents. Actually, mantle eclogite originated from the subduction can be modified by partial melting and reaction with the surrounding peridotite to form low-Fe eclogite (e.g., Smit et al., 2014; Yaxley & Green, 1998). Therefore, based on this study, the density anomalies with different values in the upper mantle of Asia can be explained by eclogites with various Fe contents.

5. Conclusions

The thermoelastic parameters of eclogitic garnets (low-Fe: $Prp_{28}Alm_{38}Grs_{33}Sps_1$ and high-Fe: $Prp_{14}Alm_{62}Grs_{19}Adr_3Sps_2$) and omphacites (low-Fe: $Quad_{57}Jd_{42}Ae_1$ and High-Fe: $Quad_{53}Jd_{27}Ae_{20}$) were obtained by fitting the *P-V-T* data to the HT-BM-EoS. The results were compared with those of previous studies. The eclogitic garnets have smaller K_0 values than end-member garnets Prp, Alm, and Grs, which may result from the excess volume induced by the incorporation of Grs. Unlike the Prp-Alm solid solution, which has K_0 values increase with increasing Alm content, the compositional dependence of K_0 values for Prp-Alm-Grs garnets is complicated. For Prp-Alm-Grs solutions, increasing Alm content may lower the thermal expansion. The K_0 values of omphacite generally increase with increasing Jd content. On the contrary, increasing Ae content may enhance the thermal expansion. The thermoelastic parameters were used to model the densities of eclogite at *P-T* conditions of the subducted oceanic crust and the normal upper mantle. Eclogite would contribute to the driving force for the slab subduction to the transition zone. However, the presence of metastable low-Fe eclogite may contribute to the slab stagnation within the upper range of the transition zone. Additionally, eclogites can explain the density anomalies at depths of 100–200 km in the upper mantle of Asia.

Acknowledgments
We acknowledge Sergey N. Tkachev for the gas loading assistance. This project was supported by the National Natural Science Foundation of China (Grant Nos. 41772043, 41374107, and 41802043), the Joint Research Fund in Huge Scientific Equipment (U1632112) under cooperative agreement between NSFC and CAS, the Chinese Academy of Sciences "Light of West China" Program (Dawei Fan, 2017), the Strategic Priority Research Program (B) of the Chinese Academy of Sciences (XDB 18010401), the China Postdoctoral Science Foundation (Grant No. 2018M631104), the Youth Innovation Promotion Association CAS (Dawei Fan, 2018434), the CPSF-CAS Joint Foundation for Excellent Postdoctoral Fellows (Grant No. 2017LH014), and the National Science Foundation under Grant EAR1722969. The experimental work was conducted at GeoSoilEnviroCARS (Sector 13), Partnership for Extreme Crystallography program (PX^2), Advanced Photon Source (APS), and Argonne National Laboratory. GeoSoilEnviroCARS is supported by the National Science Foundation—Earth Sciences (EAR-1128799) and Department of Energy—Geosciences (DE-FG02-94ER14466). PX^2 program is supported by COMPRES under NSF Cooperative Agreement EAR 11-57758. Use of the COMPRES-GSECARS gas loading system was supported by COMPRES under NSF Cooperative Agreement EAR 11-57758 and by GSECARS. Development of the ATREX software used for data analysis is supported by NSF Grant EAR1440005. Use of the Advanced Photon Source was supported by the U.S. Department of Energy, Office of Science, Office of Basic Energy Sciences, under Contract No. DE-AC02-06CH11357. We would like to thank two anonymous reviewers for their thorough and helpful comments and Jeroen Ritsema for handling this paper. Readers can access the additional data in the supporting information.

References

Agrusta, R., Hunen, J., & Goes, S. (2014). The effect of metastable pyroxene on the slab dynamics. *Geophysical Research Letters*, *41*, 8800–8808. https://doi.org/10.1002/2014GL062159

Akaogi, M., & Akimoto, S. (1977). Pyroxene-garnet solid-solution equilibria in the systems $Mg_4Si_4O_{12}$-$Mg_3Al_2Si_3O_{12}$ and $Fe_4Si_4O_{12}$-$Fe_3Al_2Si_3O_{12}$ at high pressures and temperatures. *Physics of the Earth and Planetary Interiors*, *15*(1), 90–106. https://doi.org/10.1016/0031-9201(77)90013-9

Anderson, D. L. (2006). Speculations on the nature and cause of mantle heterogeneity. *Tectonophysics*, *416*(1-4), 7–22. https://doi.org/10.1016/j.tecto.2005.07.011

Angel, R. J. (2000). Equations of state. *Reviews in Mineralogy and Geochemistry*, *41*(1), 35–59. https://doi.org/10.2138/rmg.2000.41.2

Angel, R. J., Bujak, M., Zhao, J., Gatta, G. D., & Jacobsen, S. D. (2007). Effective hydrostatic limits of pressure media for high-pressure crystallographic studies. *Journal of Applied Crystallography*, *40*(1), 26–32. https://doi.org/10.1107/S0021889806045523

Angel, R. J., Gonzalez-Platas, J., & Alvaro, M. (2014). EosFit7c and a Fortran module (library) for equation of state calculations. *Zeitschrift Fur Kristallographie*, *229*(5), 405–419.

Aoki, I., & Takahashi, E. (2004). Density of MORB eclogite in the upper mantle. *Physics of the Earth and Planetary Interiors*, *143-144*(supplement C), 129–143.

Arimoto, T., Gréaux, S., Irifune, T., Zhou, C., & Higo, Y. (2015). Sound velocities of $Fe_3Al_2Si_3O_{12}$ almandine up to 19 GPa and 1700 K. *Physics of the Earth and Planetary Interiors*, *246*, 1–8. https://doi.org/10.1016/j.pepi.2015.06.004

Babuška, V., Fiala, J., Kumazawa, M., Ohno, I., & Sumino, Y. (1978). Elastic properties of garnet solid-solution series. *Physics of the Earth and Planetary Interiors*, *16*(2), 157–176. https://doi.org/10.1016/0031-9201(78)90086-9

Bass, J. D. (1986). Elasticity of uvarovite and andradite garnets. *Journal of Geophysical Research*, *91*, 7505–7516. https://doi.org/10.1029/JB091iB07p07505

Bass, J. D. (1989). Elasticity of grossular and spessartite garnets by Brillouin spectroscopy. *Journal of Geophysical Research*, *94*, 7621–7628. https://doi.org/10.1029/JB094iB06p07621

Bass, J. D., & Anderson, D. L. (1984). Composition of the upper mantle: Geophysical tests of two petrological models. *Geophysical Research Letters*, *11*, 229–232. https://doi.org/10.1029/GL011i003p00229

Bass, J. D., Liebermann, R. C., Weidner, D. J., & Finch, S. J. (1981). Elastic properties from acoustic and volume compression experiments. *Physics of the Earth and Planetary Interiors*, *25*(2), 140–158. https://doi.org/10.1016/0031-9201(81)90147-3

Bass, J. D., & Parise, J. B. (2008). Deep Earth and recent developments in mineral physics. *Elements*, *4*(3), 157–163. https://doi.org/10.2113/GSELEMENTS.4.3.157

Bhagat, S. S., Bass, J. D., & Smyth, J. R. (1992). Single-crystal elastic properties of omphacite-C2/c by Brillouin spectroscopy. *Journal of Geophysical Research*, *97*, 6843–6848. https://doi.org/10.1029/92JB00030

Cammarano, F., Goes, S., Vacher, P., & Giardini, D. (2003). Inferring upper-mantle temperatures from seismic velocities. *Physics of the Earth and Planetary Interiors*, *138*(3–4), 197–222. https://doi.org/10.1016/S0031-9201(03)00156-0

Chen, G., Cooke, J. A., Gwanmesia, G. D., & Liebermann, R. C. (1999). Elastic wave velocities of $Mg_3Al_2Si_3O_{12}$-pyrope garnet to 10 GPa. *American Mineralogist*, *84*(3), 384–388. https://doi.org/10.2138/am-1999-0322

Dera, P., Zhuravlev, K., Prakapenka, V., Rivers, M. L., Finkelstein, G. J., Grubor-Urosevic, O., et al. (2013). High pressure single-crystal micro X-ray diffraction analysis with GSE_ADA/RSV software. *High Pressure Research*, *33*(3), 466–484. https://doi.org/10.1080/08957959.2013.806504

Du, W., Clark, S. M., & Walker, D. (2015). Thermo-compression of pyrope-grossular garnet solid solutions: Non-linear compositional dependence. *American Mineralogist*, *100*(1), 215–222. https://doi.org/10.2138/am-2015-4752

Duffy, T. S., & Anderson, D. L. (1989). Seismic velocities in mantle minerals and the mineralogy of the upper mantle. *Journal of Geophysical Research*, *94*, 1895–1912. https://doi.org/10.1029/JB094iB02p01895

Dziewonski, A. M., & Anderson, D. L. (1981). Preliminary reference Earth model. *Physics of the Earth and Planetary Interiors*, *25*(4), 297–356. https://doi.org/10.1016/0031-9201(81)90046-7

Eberle, M. A., Grasset, O., & Sotin, C. (2002). A numerical study of the interaction between the mantle wedge, subducting slab, and overriding plate. *Physics of the Earth and Planetary Interiors*, *134*(3-4), 191–202. https://doi.org/10.1016/S0031-9201(02)00157-7

Fan, D., Kuang, Y., Xu, J., Li, B., Zhou, W., & Xie, H. (2017). Thermoelastic properties of grossular–andradite solid solution at high pressures and temperatures. *Physics and Chemistry of Minerals*, *44*(2), 137–147. https://doi.org/10.1007/s00269-016-0843-4

Fan, D., Wei, S., Liu, J., & LI, Y., & Xie, H. (2011). High pressure X-ray diffraction study of a grossular–andradite solid solution and the bulk modulus variation along this solid solution. *Chinese Physics Letters*, *28*(7), 076101. https://doi.org/10.1088/0256-307X/28/7/076101

Fan, D., Xu, J., Ma, M., Liu, J., & Xie, H. (2015). *P-V-T* equation of state of spessartine-almandine solid solution measured using a diamond anvil cell and in situ synchrotron X-ray diffraction. *Physics and Chemistry of Minerals*, *42*(1), 63–72. https://doi.org/10.1007/s00269-014-0700-2

Fan, D., Xu, J., Ma, M., Wei, S., Zhang, B., Liu, J., & Xie, H. (2015). *P-V-T* equation of state of $Ca_3Cr_2Si_3O_{12}$ uvarovite garnet by using a diamond-anvil cell and in-situ synchrotron X-ray diffraction. *American Mineralogist*, *100*(2–3), 588–597. https://doi.org/10.2138/am-2015-5002

Fei, Y., Ricolleau, A., Frank, M., Mibe, K., Shen, G., & Prakapenka, V. (2007). Toward an internally consistent pressure scale. *Proceedings of the National Academy of Sciences of the United States of America*, *104*(22), 9182–9186. https://doi.org/10.1073/pnas.0609013104

Fleet, M. E., Herzberg, C. T., Bancroft, G. M., & Aldridge, L. P. (1978). Omphacite studies, I. The *P2/n–>C2/c* transformation. *American Mineralogist*, *63*, 1100–1106.

Frost, D. J. (2008). The upper mantle and transition zone. *Elements*, *4*(3), 171–176. https://doi.org/10.2113/GSELEMENTS.4.3.171

Fukao, Y., & Obayashi, M. (2013). Subducted slabs stagnant above, penetrating through, and trapped below the 660 km discontinuity. *Journal of Geophysical Research: Solid Earth*, *118*, 5920–5938. https://doi.org/10.1002/2013JB010466

Fukao, Y., Widiyantoro, S., & Obayashi, M. (2001). Stagnant slabs in the upper and lower mantle transition region. *Reviews of Geophysics*, *39*, 291–323. https://doi.org/10.1029/1999RG000068

Ganguly, J., Cheng, W., & O'Neill, H. S. C. (1993). Syntheses, volume, and structural changes of garnets in the pyrope-grossular join: Implications for stability and mixing properties. *American Mineralogist*, *78*(5–6), 583–593.

Gavrilenko, P., Ballaran, T. B., & Keppler, H. (2010). The effect of Al and water on the compressibility of diopside. *American Mineralogist*, *95*(4), 608–616. https://doi.org/10.2138/am.2010.3400

Geiger, C. A. (2013). Garnet: A key phase in nature, the laboratory, and technology. *Elements*, *9*(6), 447–452. https://doi.org/10.2113/gselements.9.6.447

Geiger, C. A., Newton, R. C., & Kleppa, O. J. (1987). Enthalpy of mixing of synthetic almandine-grossular and almandine-pyrope garnets from high-temperature solution calorimetry. *Geochimica et Cosmochimica Acta*, *51*(6), 1755–1763. https://doi.org/10.1016/0016-7037(87)90353-X

Gonzalez-Platas, J., Alvaro, M., Nestola, F., & Angel, R. (2016). EosFit7-GUI: A new graphical user interface for equation of state calculations, analyses and teaching. *Journal of Applied Crystallography*, *49*(4), 1377–1382. https://doi.org/10.1107/S1600576716008050

Gréaux, S., Kono, Y., Nishiyama, N., Kunimoto, T., Wada, K., & Irifune, T. (2011). *P–V–T* equation of state of $Ca_3Al_2Si_3O_{12}$ grossular garnet. *Physics and Chemistry of Minerals*, *38*(2), 85–94. https://doi.org/10.1007/s00269-010-0384-1

Gwanmesia, G. D., Zhang, J., Darling, K., Kung, J., Li, B., Wang, L., et al. (2006). Elasticity of polycrystalline pyrope ($Mg_3Al_2Si_3O_{12}$) to 9 GPa and 1000 °C. *Physics of the Earth and Planetary Interiors*, *155*(3-4), 179–190. https://doi.org/10.1016/j.pepi.2005.10.008

Hill, R. (1952). The elastic behavior of a crystalline aggregate. *Proceedings of the Physical Society, Section A*, *65*(5), 349–354. https://doi.org/10.1088/0370-1298/65/5/307

Hu, Y., Wu, Z., Dera, P. K., & Bina, C. R. (2016). Thermodynamic and elastic properties of pyrope at high pressure and high temperature by first-principles calculations. *Journal of Geophysical Research: Solid Earth*, *121*, 6462–6476. https://doi.org/10.1002/2016JB013026

Huang, S., & Chen, J. H. (2014). Equation of state of pyrope-almandine solid solution measured using a diamond anvil cell and in situ synchrotron X-ray diffraction. *Physics of the Earth and Planetary Interiors*, *228*, 88–91. https://doi.org/10.1016/j.pepi.2014.01.014

Irifune, T., Sekine, T., Ringwood, A., & Hibberson, W. (1986). The eclogite-garnetite transformation at high pressure and some geophysical implications. *Earth and Planetary Science Letters*, *77*(2), 245–256. https://doi.org/10.1016/0012-821X(86)90165-2

Isaak, D. G., Anderson, O. L., & Oda, H. (1992). High-temperature thermal expansion and elasticity of calcium-rich garnets. *Physics and Chemistry of Minerals*, *19*(2), 106–120.

Jacob, D. E. (2004). Nature and origin of eclogite xenoliths from kimberlites. *Lithos*, *77*(1-4), 295–316. https://doi.org/10.1016/j.lithos.2004.03.038

Jiang, F., Speziale, S., & Duffy, T. S. (2004). Single-crystal elasticity of grossular-and almandine-rich garnets to 11 GPa by Brillouin scattering. *Journal of Geophysical Research*, *109*, B10210. https://doi.org/10.1029/2004JB003081

John, K., & Weidner, D. J. (1988). Elastic properties of hedenbergite. *Journal of Geophysical Research*, *93*, 1063–1072. https://doi.org/10.1007/s002690050156

Kaban, M. K., Khrepy, S. E., Al-Arifi, N., Tesauro, M., & Stolk, W. (2016). Three-dimensional density model of the upper mantle in the Middle East: Interaction of diverse tectonic processes. *Journal of Geophysical Research: Solid Earth*, *121*, 5349–5364. https://doi.org/10.1002/2015JB012755

Kaban, M. K., Stolk, W., Tesauro, M., El Khrepy, S., Al-Arifi, N., Beekman, F., & Cloetingh, S. A. (2016). 3D density model of the upper mantle of Asia based on inversion of gravity and seismic tomography data. *Geochemistry, Geophysics, Geosystems*, *17*, 4457–4477. https://doi.org/10.1002/2016GC006458

Kandelin, J., & Weidner, D. J. (1988). The single-crystal elastic properties of jadeite. *Physics of the Earth and Planetary Interiors*, *50*(3), 251–260. https://doi.org/10.1016/0031-9201(88)90106-9

Kantor, I., Prakapenka, V., Kantor, A., Dera, P., Kurnosov, A., Sinogeikin, S., et al. (2012). BX90: A new diamond anvil cell design for X-ray diffraction and optical measurements. *Review of Scientific Instruments*, *83*(12), 125102. https://doi.org/10.1063/1.4768541

Katsura, T., Yoneda, A., Yamazaki, D., Yoshino, T., & Ito, E. (2010). Adiabatic temperature profile in the mantle. *Physics of the Earth and Planetary Interiors*, *183*(1–2), 212–218. https://doi.org/10.1016/j.pepi.2010.07.001

Kono, Y., Greaux, S., Higo, Y., Ohfuji, H., & Irifune, T. (2010). Pressure and temperature dependences of elastic properties of grossular garnet up to 17 GPa and 1 650 K. *Journal of Earth Science*, *21*(5), 782–791.

Kosman, C. W., Kopylova, M. G., Stern, R. A., Hagadorn, J. W., & Hurlbut, J. F. (2016). Cretaceous mantle of the Congo craton: Evidence from mineral and fluid inclusions in Kasai alluvial diamonds. *Lithos*, *265*(Supplement C), 42–56.

Koziol, A. M., & Newton, R. C. (1989). Grossular activity-composition relationships in ternary garnets determined by reversed displaced-equilibrium experiments. *Contributions to Mineralogy and Petrology*, *103*(4), 423–433. https://doi.org/10.1007/BF01041750

Leitner, B. J., Weidner, D. J., & Liebermann, R. C. (1980). Elasticity of single crystal pyrope and implications for garnet solid solution series. *Physics of the Earth and Planetary Interiors*, *22*(2), 111–121. https://doi.org/10.1016/0031-9201(80)90052-7

Levien, L., & Prewitt, C. T. (1981). High-pressure structural study of diopside. *American Mineralogist*, *66*(3–4), 315–323.

Levien, L., Prewitt, C. T., & Weidner, D. J. (1979). Compression of pyrope. *American Mineralogist*, *64*, 805–808.

Li, B., & Neuville, D. R. (2010). Elasticity of diopside to 8 GPa and 1073 K and implications for the upper mantle. *Physics of the Earth and Planetary Interiors*, *183*(3-4), 398–403. https://doi.org/10.1016/j.pepi.2010.08.009

Lu, C., Mao, Z., Lin, J.-F., Zhuravlev, K. K., Tkachev, S. N., & Prakapenka, V. B. (2013). Elasticity of single-crystal iron-bearing pyrope up to 20 GPa and 750 K. *Earth and Planetary Science Letters*, *361*, 134–142. https://doi.org/10.1016/j.epsl.2012.11.041

McCarthy, A. C., Downs, R. T., & Thompson, R. M. (2008). Compressibility trends of the clinopyroxenes, and in-situ high-pressure single-crystal X-ray diffraction study of jadeite. *American Mineralogist*, *93*(1), 198–209. https://doi.org/10.2138/am.2008.2521

McCarthy, A. C., Downs, R. T., Thompson, R. M., & Redhammer, G. J. (2008). In situ high-pressure single-crystal X-ray study of aegirine, $NaFe^{3+}Si_2O_6$, and the role of M1 size in clinopyroxene compressibility. *American Mineralogist*, *93*(11–12), 1829–1837. https://doi.org/10.2138/am.2008.2725

Milani, S. (2015). Compressibility and thermal expansion of garnets with compositions typical of inclusions in diamonds, PhD thesis, Università degli Studi di Padova.

Milani, S., Nestola, F., Alvaro, M., Pasqual, D., Mazzucchelli, M. L., Domeneghetti, M. C., & Geiger, C. A. (2015). Diamond-garnet geobarometry: The role of garnet compressibility and expansivity. *Lithos*, *227*, 140–147. https://doi.org/10.1016/j.lithos.2015.03.017

Mooney, W. D., & Kaban, M. K. (2010). The North American upper mantle: Density, composition, and evolution. *Journal of Geophysical Research*, *115*, B12424. https://doi.org/10.1029/2010JB000866

Morimoto, N. (1988). Nomenclature of pyroxenes. *Mineralogy and Petrology*, *39*(1), 55–76. https://doi.org/10.1007/BF01226262

Nestola, F., Ballaran, T. B., Liebske, C., Bruno, M., & Tribaudino, M. (2006). High-pressure behaviour along the jadeite $NaAlSi_2O_6$-aegirine $NaFeSi_2O_6$ solid solution up to 10 GPa. *Physics and Chemistry of Minerals*, *33*(6), 417–425. https://doi.org/10.1007/s00269-006-0089-7

Nishi, M., Kato, T., Kubo, T., & Kikegawa, T. (2008). Survival of pyropic garnet in subducting plates. *Physics of the Earth and Planetary Interiors*, *170*(3-4), 274–280. https://doi.org/10.1016/j.pepi.2008.03.013

Nishi, M., Kubo, T., & Kato, T. (2009). Metastable transformations of eclogite to garnetite in subducting oceanic crust. *Journal of Mineralogical and Petrological Sciences*, *104*(3), 192–198. https://doi.org/10.2465/jmps.080929

Nishi, M., Kubo, T., Ohfuji, H., Kato, T., Nishihara, Y., & Irifune, T. (2013). Slow Si–Al interdiffusion in garnet and stagnation of subducting slabs. *Earth and Planetary Science Letters*, *361*, 44–49. https://doi.org/10.1016/j.epsl.2012.11.022

Nishihara, Y., Takahashi, E., Matsukage, K., & Kikegawa, T. (2003). Thermal equation of state of omphacite. *American Mineralogist*, *88*(1), 80–86. https://doi.org/10.2138/am-2003-0110

O'Neill, B., Bass, J. D., Rossman, G. R., Geiger, C. A., & Langer, K. (1991). Elastic properties of pyrope. *Physics and Chemistry of Minerals*, *17*(7), 617–621.

Pandolfo, F., Nestola, F., Camara, F., & Domeneghetti, M. C. (2012a). High-pressure behavior of space group P2/n omphacite. *American Mineralogist*, *97*(2–3), 407–414. https://doi.org/10.2138/am.2012.3928

Pandolfo, F., Nestola, F., Cámara, F., & Domeneghetti, M. C. (2012b). New thermoelastic parameters of natural *C*2/*c* omphacite. *Physics and Chemistry of Minerals*, *39*(4), 295–304. https://doi.org/10.1007/s00269-012-0484-1

Pavese, A., Diella, V., Levy, D., & Hanfland, M. (2001). Synchrotron X-ray powder diffraction study of natural *P*2/*n*-omphacites at high-pressure conditions. *Physics and Chemistry of Minerals*, *28*(1), 9–16. https://doi.org/10.1007/s002690000128

Posner, E. S., Dera, P., Downs, R. T., Lazarz, J. D., & Irmen, P. (2014). High-pressure single-crystal X-ray diffraction study of jadeite and kosmochlor. *Physics and Chemistry of Minerals*, *41*(9), 695–707. https://doi.org/10.1007/s00269-014-0684-y

Ren, Y., Chen, D., Kelsey, D. E., Gong, X., & Liu, L. (2017). Petrology and geochemistry of the lawsonite (pseudomorph)-bearing eclogite in Yuka terrane, North Qaidam UHPM belt: An eclogite facies metamorphosed oceanic slice. *Gondwana Research*, *42*(Supplement C), 220–242.

Ringwood, A. E. (1982). Phase transformations and differentiation in subducted lithosphere: Implications for mantle dynamics, basalt petrogenesis, and crustal evolution. *The Journal of Geology*, *90*(6), 611–643. https://doi.org/10.1086/628721

Rivers, M., Prakapenka, V. B., Kubo, A., Pullins, C., Holl, C. M., & Jacobsen, S. D. (2008). The COMPRES/GSECARS gas-loading system for diamond anvil cells at the Advanced Photon Source. *High Pressure Research*, *28*(3), 273–292. https://doi.org/10.1080/08957950802333593

Sang, L., & Bass, J. D. (2014). Single-crystal elasticity of diopside to 14 GPa by Brillouin scattering. *Physics of the Earth and Planetary Interiors*, *228*, 75–79. https://doi.org/10.1016/j.pepi.2013.12.011

Shannon, R. (1976). Revised effective ionic radii and systematic studies of interatomic distances in halides and chalcogenides. *Acta Crystallographica, Section A: Crystal Physics, Diffraction, Theoretical and General Crystallography*, *32*(5), 751–767. https://doi.org/10.1107/S0567739476001551

Sinogeikin, S. V., & Bass, J. D. (2000). Single-crystal elasticity of pyrope and MgO to 20 GPa by Brillouin scattering in the diamond cell. *Physics of the Earth and Planetary Interiors*, *120*(1-2), 43–62. https://doi.org/10.1016/S0031-9201(00)00143-6

Sinogeikin, S. V., & Bass, J. D. (2002). Elasticity of pyrope and majorite–pyrope solid solutions to high temperatures. *Earth and Planetary Science Letters*, *203*(1), 549–555. https://doi.org/10.1016/S0012-821X(02)00851-8

Skinner, B. J. (1956). Physical properties of end-members of the garnet group. *American Mineralogist*, *41*(5–6), 428–436.

Smit, K., Stachel, T., Creaser, R., Ickert, R., DuFrane, S., Stern, R., & Seller, M. (2014). Origin of eclogite and pyroxenite xenoliths from the Victor kimberlite, Canada, and implications for Superior craton formation. *Geochimica et Cosmochimica Acta*, *125*, 308–337. https://doi.org/10.1016/j.gca.2013.10.019

Soga, N. (1967). Elastic constants of garnet under pressure and temperature. *Journal of Geophysical Research*, *72*, 4227–4234. https://doi.org/10.1029/JZ072i016p04227

Stachel, T., & Harris, J. W. (2008). The origin of cratonic diamonds—Constraints from mineral inclusions. *Ore Geology Reviews*, *34*(1-2), 5–32. https://doi.org/10.1016/j.oregeorev.2007.05.002

Stixrude, L., & Lithgow-Bertelloni, C. (2011). Thermodynamics of mantle minerals—II. Phase equilibria. *Geophysical Journal International*, *184*(3), 1180–1213.

Sumino, Y., & Nishizawa, O. (1978). Temperature variation of elastic constants of pyrope-almandine garnets. *Journal of Physics of the Earth*, *26*(3), 239–252. https://doi.org/10.4294/jpe1952.26.239

Taylor, L. A., Snyder, G. A., Crozaz, G., Sobolev, V. N., Yefimova, E. S., & Sobolev, N. V. (1996). Eclogitic inclusions in diamonds: Evidence of complex mantle processes over time. *Earth and Planetary Science Letters*, *142*(3-4), 535–551. https://doi.org/10.1016/0012-821X(96)00106-9

Thompson, R. M., & Downs, R. T. (2008). The crystal structure of diopside at pressure to 10 GPa. *American Mineralogist*, *93*(1), 177–186. https://doi.org/10.2138/am.2008.2684

Tribaudino, M., Nestola, F., Bruno, M., Ballaran, T. B., & Liebske, C. (2008). Thermal expansion along the $NaAlSi_2O_6$-$NaFe^{3+}Si_2O_6$ and $NaAlSi_2O_6$-$CaFe^{2+}Si_2O_6$ solid solutions. *Physics and Chemistry of Minerals*, *35*(5), 241–248. https://doi.org/10.1007/s00269-008-0217-7

Van Mierlo, W., Langenhorst, F., Frost, D., & Rubie, D. (2013). Stagnation of subducting slabs in the transition zone due to slow diffusion in majoritic garnet. *Nature Geoscience*, *6*(5), 400–403. https://doi.org/10.1038/ngeo1772

Verma, R. K. (1960). Elasticity of some high-density crystals. *Journal of Geophysical Research*, *65*, 757–766. https://doi.org/10.1029/JZ065i002p00757

Vinet, P., Ferrante, J., Smith, J. R., & Rose, J. H. (1986). A universal equation of state for solids. *Journal of Physics C: Solid State Physics*, *19*(20), L467–L473. https://doi.org/10.1088/0022-3719/19/20/001

Wang, R., Wang, S., Qiu, J., & Ni, P. (2009). Characterization of high-Ti eclogitic garnets in the Dabie-Sulu ultrahigh-pressure metamorphic belt (China): Compositional heterogeneity and possible relations to rutile needles in garnet (in Chinese). *Acta Petrologica Sinica*, *25*(7), 1603–1611.

Wang, W. (1998). Formation of diamond with mineral inclusions of "mixed" eclogite and peridotite paragenesis. *Earth and Planetary Science Letters*, *160*(3-4), 831–843. https://doi.org/10.1016/S0012-821X(98)00131-9

Wang, Y., Weidner, D. J., Zhang, J., Gwanrnesia, G. D., & Liebermann, R. C. (1998). Thermal equation of state of garnets along the pyrope-majorite join. *Physics of the Earth and Planetary Interiors*, *105*(1-2), 59–71. https://doi.org/10.1016/S0031-9201(97)00072-1

Webb, S. L. (1989). The elasticity of the upper mantle orthosilicates olivine and garnet to 3 GPa. *Physics and Chemistry of Minerals*, *16*(7), 684–692.

Weber, S., & Bucher, K. (2015). An eclogite-bearing continental tectonic slice in the Zermatt–Saas high-pressure ophiolites at Trockener Steg (Zermatt, Swiss Western Alps). *Lithos*, *232*(Supplement C), 336–359.

Xu, J., Zhang, D., Fan, D., Downs, R. T., Hu, Y., & Dera, P. (2017). Isosymmetric pressure-induced bonding increase changes compression behavior of clinopyroxenes across jadeite-aegirine solid solution in subduction zones. *Journal of Geophysical Research: Solid Earth*, *122*, 142–157. https://doi.org/10.1002/2016JB013502

Yaxley, G. M., & Green, D. H. (1998). Reactions between eclogite and peridotite: Mantle refertilisation by subduction of oceanic crust. *Schweizerische Mineralogische und Petrographische Mitteilungen*, *78*(2), 243–255.

Zhang, D., Dera, P. K., Eng, P. J., Stubbs, J. E., Zhang, J. S., Prakapenka, V. B., & Rivers, M. L. (2017). High pressure single crystal diffraction at PX^2. *Journal of Visualized Experiments*, *119*, e54660.

Zhang, D., Hu, Y., & Dera, P. K. (2016). Compressional behavior of omphacite to 47 GPa. *Physics and Chemistry of Minerals*, *43*(10), 707–715. https://doi.org/10.1007/s00269-016-0827-4

Zhang, L., Ahsbahs, H., Hafner, S. S., & Kutoglu, A. (1997). Single-crystal compression and crystal structure of clinopyroxene up to 10 GPa. *American Mineralogist*, *82*(3-4), 245–258. https://doi.org/10.2138/am-1997-3-402

Zhang, L., Ahsbahs, H., Kutoglu, A., & Geiger, C. A. (1999). Single-crystal hydrostatic compression of synthetic pyrope, almandine, spessartine, grossular and andradite garnets at high pressures. *Physics and Chemistry of Minerals*, *27*(1), 52–58. https://doi.org/10.1007/s002690050240

Zhao, Y., Dreele, R. V., Zhang, J., & Weidner, D. (1998). Thermoelastic equation of state of monoclinic pyroxene: $CaMgSi_2O_6$ diopside. *The Review of High Pressure Science and Technology*, *7*, 25–27. https://doi.org/10.4131/jshpreview.7.25

Zhao, Y., Von Dreele, R. B., Shankland, T. J., Weidner, D. J., Zhang, J., Wang, Y., & Gasparik, T. (1997). Thermoelastic equation of state of jadeite $NaAlSi_2O_6$: An energy-dispersive Reitveld Refinement Study of low symmetry and multiple phases diffraction. *Geophysical Research Letters*, *24*, 5–8. https://doi.org/10.1029/96GL03769

Zou, Y., Gréaux, S., Irifune, T., Whitaker, M. L., Shinmei, T., & Higo, Y. (2012). Thermal equation of state of $Mg_3Al_2Si_3O_{12}$ pyrope garnet up to 19 GPa and 1,700 K. *Physics and Chemistry of Minerals*, *39*(7), 589–598. https://doi.org/10.1007/s00269-012-0514-z